

- C. Pritchett, Eds. (Astronomical Society of the Pacific, Provo, UT, 1988), p. 231.
10. A. Sandage and G. Tammann, *Astrophys. J.* **256**, 339 (1982).
 11. P. Hodge, *Annu. Rev. Astron. Astrophys.* **19**, 357 (1981); M. Rowan-Robinson, *Space Sci. Rev.* **48**, 1 (1988). See also the conference proceedings *Galaxy Distances and Deviations From Universal Expansion*, B. Madore and R. B. Tully, Eds. (Reidel, Dordrecht, Netherlands, 1986), and *The Extragalactic Distance Scale*, 100th Astronomical Society of the Pacific Anniversary Symposium, S. van den Bergh and C. Pritchett, Eds. (Astronomical Society of the Pacific, Provo, UT, 1988).
 12. D. Overbye, *Lonely Hearts of the Cosmos* (Harper Collins, New York, 1991).
 13. K. Malmquist, *Medd. Lund. Astron. Obs. Ser. 2* (no. 22) (1920); P. Teerikorpi, *Astron. Astrophys.* **45**, 117 (1975); E. Giraud, *Astrophys. J.* **301**, 7 (1986); L. Bottinelli, L. Gouguenheim, G. Paturel, P. Teerikorpi, *Astron. Astrophys.* **156**, 167 (1986).
 14. A. Sandage, *Astrophys. J.* **331**, 605 (1988).
 15. R. B. Tully, *Nature* **334**, 209 (1988).
 16. G. de Vaucouleurs, *Astron. J.* **63**, 253 (1958).
 17. For example, E. Cheng, P. Saulson, D. Wilkinson, B. Corey, *Astrophys. J. Lett.* **232**, L139 (1979).
 18. P. Schechter, *Astron. J.* **85**, 801 (1980); J. Tonry and M. Davis, *Astrophys. J.* **246**, 680 (1981); M. Aaronson et al., *ibid.* **258**, 64 (1982).
 19. M. Aaronson et al., *Astrophys. J.* **302**, 536 (1986); A. Dressler et al., *Astrophys. J. Lett.* **313**, L37 (1987); D. Lynden-Bell et al., *Astrophys. J.* **326**, 19 (1988). The last two papers describe the discovery of a large mass concentration at perhaps four times the Virgo Cluster distance, now called the "Great Attractor."
 20. G. Bothun, M. West, J. Mould, R. Schommer, *Astrophys. J.* **353**, 344 (1990).
 21. A. Sandage and J. M. Perlemuter, *ibid.* **370**, 455 (1991).
 22. I. E. Segal, *Proc. Natl. Acad. Sci. U.S.A.* **72**, 2473 (1975); *ibid.* **77**, 10 (1980).
 23. K. Cook, M. Aaronson, G. Illingworth, *Astrophys. J. Lett.* **301**, L45 (1986), Cepheids in M101; W. Freedman and B. Madore, *ibid.* **332**, L63 (1988), Cepheids in M81 and NGC 2403.
 24. W. Freedman, *ibid.* **355**, L35 (1990).
 25. M. Pierce and R. B. Tully, *Astrophys. J.* **387**, 47 (1992); M. Capaccioli, G. Plotto, F. Bresolin, *Astron. J.* **103**, 1151 (1992).
 26. J. Tonry and D. Schneider, *Astron. J.* **96**, 807 (1988).
 27. J. Tonry, E. Ajhar, G. Luppino, *Astrophys. J. Lett.* **346**, L57 (1989); J. Tonry, *ibid.* **373**, L1 (1991).
 28. G. Jacoby, *Astrophys. J.* **339**, 39 (1989).
 29. R. Ciardullo et al., *ibid.* **383**, 487 (1991); G. Jacoby et al., *ibid.* **356**, 332 (1990).
 30. B. Schmidt, R. Kirshner, R. Eastman, *ibid.*, in press.
 31. D. Branch, in *The Extragalactic Distance Scale*, S. van den Bergh and C. Pritchett, Eds. (Astronomical Society of the Pacific, Provo, UT, 1988), p. 146.
 32. M. Fukugita and C. Hogan, *Astrophys. J. Lett.* **368**, L11 (1991).
 33. M. Pierce, M. Ressler, M. Shure, *Astrophys. J.*, in press.
 34. C. Pritchett and S. van den Bergh, *ibid.* **318**, 507 (1987).
 35. A. Sandage and G. Tammann, *ibid.* **328**, 1 (1988).
 36. M. Aaronson et al., *ibid.* **338**, 654 (1989); J. Mould et al., *ibid.* **383**, 467 (1991); J. Willick, *ibid.* **351**, L5 (1990).
 37. S. Faber and D. Burstein, in *Large Scale Motions in the Universe*, G. V. Coyne and V. Rubin, Eds. (Vatican Press, Rome, 1988), p. 116.
 38. D. Mathewson, V. Ford, M. Buchhorn, *Astrophys. J.*, in press.
 39. M. Rowan-Robinson et al., *Mon. Not. R. Astron. Soc.* **247**, 1 (1990); M. Strauss, M. Davis, A. Yahil, J. Huchra, *Astrophys. J.*, in press.
 40. E. Bertschinger, A. Dekel, S. Faber, A. Dressler, D. Burstein, *Astrophys. J.* **364**, 349 (1990).
 41. M. Birkinshaw, J. Hughes, K. Arnaud, *ibid.* **379**, 466 (1991).
 42. E. Falco et al., *ibid.* **372**, 364 (1991).
 43. G. Rhee, *Nature* **350**, 211 (1991).
 44. W. H. Press, G. Rybicki, J. N. Hewitt, *Astrophys. J.* **385**, 404 (1992).
 45. M. Pierce and R. B. Tully, *ibid.* **330**, 579 (1988).
 46. R. Kraan-Korteweg, L. Cameron, G. Tammann, *ibid.* **331**, 620 (1988).
 47. P. Fouque, L. Bottinelli, L. Gouguenheim, G. Paturel, *ibid.* **349**, 1 (1990).
 48. M. Fukugita, S. Okamura, K. Tarusawa, H. Rood, B. Williams, *ibid.* **376**, 8 (1991).
 49. A. Sandage, *ibid.* **331**, 605 (1988).
 50. J. Huchra, in *The Extragalactic Distance Scale*, S. van den Bergh and C. Pritchett, Eds. (Astronomical Society of the Pacific, Provo, UT, 1988), p. 257.
 51. M. Pierce, *Astrophys. J.* **344**, L57 (1989).
 52. A. Dressler, *ibid.* **317**, 1 (1987).
 53. R. Buta and H. Corwin, Jr., *Astron. J.* **62**, 283 (1986).
 54. G. de Vaucouleurs and H. Corwin, Jr., *Astrophys. J.* **308**, 487 (1986).
 55. A. Sandage, *ibid.* **331**, 583 (1988).
 56. M. Capaccioli et al., *ibid.* **350**, 110 (1990).
 57. J. Melnick, R. Terlevich, M. Moles, *Mon. Not. R. Astron. Soc.* **235**, 297 (1988).
 58. M. Aaronson and J. Mould, *Astrophys. J.* **303**, 1 (1986).
 59. A. Sandage and G. Tammann, *ibid.* **365**, 1 (1990).
 60. M. Rowan-Robinson, *Space Sci. Rev.* **48**, 1 (1988).
 61. S. van den Bergh, in *The Extragalactic Distance Scale*, S. van den Bergh and C. Pritchett, Eds. (Astronomical Society of the Pacific, Provo, UT, 1988), p. 375.
 62. N. Visvanathan, *Aust. J. Phys.* **43**, 189 (1990).
 63. J. Huchra, in *13th Texas Symposium on Relativistic Astrophysics*, M. Ulmer, Ed. (World Scientific, Singapore, 1987), p. 1.
 64. A. Guth, *Phys. Rev. D* **23**, 347 (1981).
 65. G. R. Blumenthal, S. M. Faber, J. R. Primack, M. J. Rees, *Nature* **311**, 517 (1984).
 66. S. Weinberg, *Rev. Mod. Phys.* **61**, 1 (1989). The cosmological constant, Λ , is a pressure term introduced by Einstein into his theory of general relativity, before he knew of the universal expansion, to allow for a static solution for the universe.
 67. J. Huchra, in *Dark Matter*, the proceedings of the first Institute for Fundamental Theory conference, in press; S. Faber and J. Gallagher, *Annu. Rev. Astron. Astrophys.* **17**, 135 (1979).
 68. P. J. E. Peebles, *Astrophys. J.* **284**, 439 (1984); G. Efstathiou, W. J. Sutherland, S. J. Maddox, *Nature* **348**, 705 (1990).
 69. E. Turner, *Astrophys. J. Lett.* **365**, L43 (1990).
 70. M. Fukugita et al., *ibid.* **361**, L1 (1990).
 71. See, for example, D. Miller and D. Branch [*Astron. J.* **100**, 530 (1990); *ibid.* **103**, 379 (1992)], who show that the dispersion for SN Ia may be as low as 0.3 magnitude.
 72. This work is dedicated to the memory of Marc Aaronson, with whom I spent many nights observing galaxies and pondering the cosmic distance scale. I also thank the Hubble Space Telescope Key Project team: J. Mould, R. Kennicutt, J. Graham, W. Freedman, B. Madore, H. Ford, J. Hoessel, P. Stetson, G. Illingworth, S. Faber, and J. Gunn, as well as B. Schmidt, R. Kirshner, and R. Schommer for thoughtful discussions. Supported in part by the National Aeronautics and Space Administration and the Smithsonian Institution.

LIGO: The Laser Interferometer Gravitational-Wave Observatory

Alex Abramovici, William E. Althouse, Ronald W. P. Drever, Yekta Gürsel, Seiji Kawamura, Frederick J. Raab, David Shoemaker, Lisa Sievers, Robert E. Spero, Kip S. Thorne, Rochus E. Vogt, Rainer Weiss, Stanley E. Whitcomb, Michael E. Zucker

The goal of the Laser Interferometer Gravitational-Wave Observatory (LIGO) Project is to detect and study astrophysical gravitational waves and use data from them for research in physics and astronomy. LIGO will support studies concerning the nature and nonlinear dynamics of gravity, the structures of black holes, and the equation of state of nuclear matter. It will also measure the masses, birth rates, collisions, and distributions of black holes and neutron stars in the universe and probe the cores of supernovae and the very early universe. The technology for LIGO has been developed during the past 20 years. Construction will begin in 1992, and under the present schedule, LIGO's gravitational-wave searches will begin in 1998.

Einstein's general relativity theory describes gravity as due to a curvature of space-time (1). When the curvature is weak, it produces the familiar Newtonian gravity that governs the solar system. When

the curvature is strong, however, it should behave in a radically different, highly nonlinear way. According to general relativity, the nonlinearity creates black holes (curvature produces curvature without the aid of any matter), governs their structure, and holds them together against disruption (2). Inside a black hole, the curvature should nonlinearly amplify itself to produce a space-time singularity (2), and near some singularities the nonlinearity should force the curvature to evolve chaotically (3). When an object's curvature varies rapidly (for example, because of pulsations, colli-

The authors are the members of the LIGO Science Steering Group. A. Abramovici, W. E. Althouse (Chief Engineer), R. W. P. Drever, S. Kawamura, F. J. Raab, L. Sievers, R. E. Spero, K. S. Thorne, R. E. Vogt (Director), S. E. Whitcomb (Deputy Director), and M. E. Zucker are with the California Institute of Technology, Pasadena, CA 91125. Y. Gürsel is at the Jet Propulsion Laboratory, Pasadena, CA 91109. D. Shoemaker and R. Weiss are at the Massachusetts Institute of Technology, Cambridge, MA 02129.

sions, or rapid orbital motions), it should emanate curvature ripples (gravitational waves) that propagate through the universe at the speed of light and carry the imprint of gravity's quantum-mechanical particle, the graviton.

This description of gravity is almost entirely theoretical and untested. Gravitational waves have never been observed directly [although the orbital decay of neutron star PSR 1913+16 shows indirectly that they exist and carry energy away from binary stars at the rate predicted by general relativity (4)]. Our only observational evidence for the nonlinearity of space-time curvature is the observation of tiny perturbations of planetary and binary star orbits (5), and these teach us nothing about the rich variety of nonlinear curvature phenomena that we expect from experience with other nonlinear systems. Moreover, although astronomers have found strong circumstantial evidence for the existence of black holes and astrophysicists invoke them to help explain astronomical observations, electromagnetic radiation has not yet brought to Earth a clean, unequivocal signature saying "I come from a black hole," and the observations have not been able to be used to test any of the predicted properties of black holes.

LIGO offers an opportunity to bring nonlinear gravity, black holes, and the graviton out of their near isolation as theoretical constructs and into confrontation with experiment. LIGO can verify that

these ripples of curvature (gravitational waves) exist. From the force patterns of the waves, LIGO can allow researchers to infer the graviton's spin (6, 7). From the difference in arrival times of electromagnetic and gravitational-wave bursts from the same distant event, LIGO can allow researchers to infer the difference in the speeds of gravitational waves and light—a difference that must be zero if (as theory predicts) the graviton has zero rest mass (7).

The shapes of a gravitational wave's oscillations (its waveforms; see Fig. 1) carry detailed information about its source, information that LIGO will extract for use in physics research. For example, the waveforms from a small black hole spiraling into a large black hole carry an unequivocal "black hole" signature, a signature that maps out, in detail, a portion of the large hole's space-time geometry (8, 9); by comparing that map with general relativity's predictions, researchers will test highly nonlinear aspects of general relativity. The waveforms from colliding black holes, when compared to those from supercomputer simulations, will give insight into the poorly understood nonlinear dynamics of gravity (10). The waveforms from colliding neutron stars or from neutron stars being torn apart by the tidal gravity of companion black holes may reveal the mass-radius relation for neutron stars, which in turn will give information about the equation of state of nuclear matter (11).

Astrophysical sources have oscillation periods ranging from many hours to less than 1 ms. LIGO is designed to detect only those signals with oscillation periods faster than about 100 ms; slower oscillations are difficult to detect with Earth-based systems because of low-frequency background disturbances. Fortunately, many potential sources have oscillation periods within LIGO's range, including neutron stars, black holes with masses of up to 10^4 solar masses, supernovae cores, and the big bang.

One can best appreciate LIGO's potential for major contributions to astronomy by recalling the history of radio astronomy (12). Before Jansky's discovery of cosmic radio waves in 1932, the universe, as viewed solely through visible light, seemed serene and quiescent, dominated by slowly evolving stars. Radio waves revolutionized this view; they revealed our universe's violent side: pulsars, quasars, active galactic nuclei, and jets that power huge intergalactic clouds of magnetized plasma.

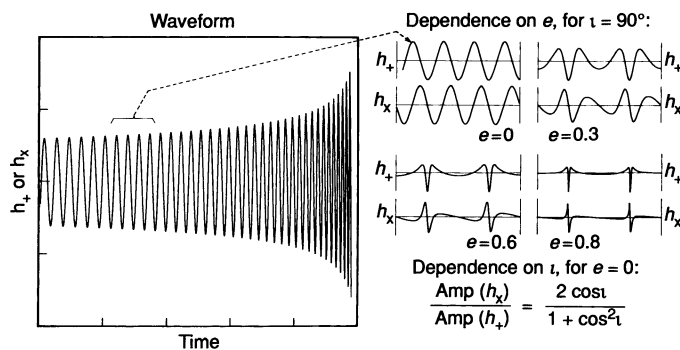
The radio revolution was spectacular because the information carried by radio waves is so different from that carried by light. Light, with its submicrometer wavelength, is emitted mostly by thermally excited atoms in the atmospheres of stars; radio waves, with their ten million-fold as large wavelengths, are emitted mostly by high-energy electrons spiraling in the magnetic fields of pulsars, quasars, or jets.

This difference between light and radio waves pales in comparison with the contrast between electromagnetic waves and gravitational waves. Electromagnetic astronomy usually monitors incoherent superpositions of radiation from individual electrons, atoms, or molecules; gravitational waves are produced most strongly by coherent, bulk motions of huge amounts of mass—either material mass or the mass-energy of nonlinear space-time curvature (7, 13). Electromagnetic waves are easily absorbed and scattered by matter; gravitational waves travel nearly unchanged through all forms and amounts of intervening matter (7).

Compared to electromagnetic telescopes, LIGO is sensitive to very different aspects of the universe. Electromagnetic telescopes study such things as stellar atmospheres, interstellar gas and dust, and primordial gas; LIGO is insensitive to these. LIGO will seek waves from the final inspiral and coalescence of binary black holes and neutron stars, the rapidly spinning cores of supernovae, and the first fraction of a second of the big bang (14); to these, electromagnetic telescopes have little or no sensitivity.

These differences produce both uncertainty and great expectations. It is hard to predict, from our present electromagnetic-based knowledge, just how sensitive detec-

Fig. 1. An example of gravitational waveforms and the information they carry. Each gravitational wave has two waveforms, dimensionless functions of time called $h_+(t)$ and $h_\times(t)$. The specific waveforms shown here (30) are from the last few minutes or seconds of the spiraling together of a compact binary system



(one made of two black holes, two neutron stars, or a black hole and a neutron star). By monitoring these waveforms, LIGO can allow researchers to determine (30) the binary's distance from Earth r , the masses of its two bodies or, equivalently, their total mass M and reduced mass μ , and their orbital eccentricity e and orbital inclination to the line of sight ι . To allow the determination of the eccentricity e , LIGO will measure the shapes of the individual waveform oscillations; note the shapes shown on the upper right. For the determination of ι (when $e = 0$ for pedagogic simplicity), LIGO will measure the ratio of the amplitudes, h_+ and h_\times ; see the formula in the lower right. The parameters r , μ , and M determine (i) the waveforms' absolute amplitudes as they sweep past a frequency f : $h_{\text{amp}} \propto \mu M^{2/3} r^{-1} f^{2/3}$; and (ii) the number of cycles $n = f^2 (df/dt)^{-1}$ that the waveforms spend near frequency f : $n \propto (\mu M^{2/3} f^{5/3})^{-1}$. From h_{amp} and n , LIGO can be used to determine r and $\mu M^{2/3}$. From $\mu M^{2/3}$, and from late-time post-Newtonian facets of the waveform (31) (not shown here) or the frequency at which the inspiral terminates or both, LIGO can be used to deduce the individual values of μ and M (8). The simple inspiral waves shown here are modified at late times by post-Newtonian (31) and then fully relativistic (8, 9) effects and then are followed by much more complicated waveforms from the final collision or tidal disruption of the black holes or neutron stars. It is these final relativistic, collision, and disruption waveforms that will bring LIGO the most interesting information.

tors in LIGO must be to detect their first waves; but once LIGO sees waves, it will bring information about the universe that we have little hope of gaining in any other way. LIGO will teach us about the universe of strongly gravitating objects, such as the masses, birth rates, and spatial distributions of black hole and neutron star binaries in the distant universe, and perhaps about the shapes of rapidly spinning neutron stars in our own galaxy, the spectrum of "cosmic strings," and the first fraction of a second of the universe's expansion (14). LIGO may well bring surprises that rival those of radio astronomy.

Laser Interferometer Gravitational-Wave Detectors

According to general relativity theory, every freely moving particle (called a test particle) travels through space-time along a geodesic, a path that is the analog of a straight line in curved space. Just as the curvature of Earth's surface pushes Earth's lines of constant longitude (its geodesics) together as one travels from the equator toward the North or South Pole, so also the curvature of space-time pushes neighboring space-time geodesics together or apart and thereby pushes test particles moving along the geodesics together or apart (1).

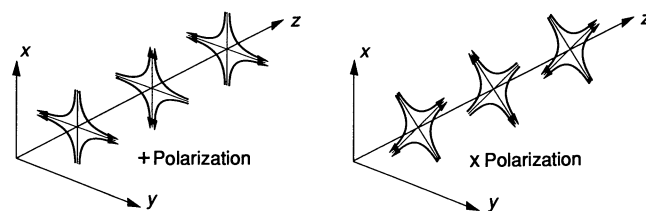
If the curvature is that of a gravitational wave, then the test particles' relative motion is a sum of contributions from two different polarizations (Fig. 2), each with its own time-evolving waveform: $h_+(t)$ and $h_\times(t)$. This relative motion of test particles is the foundation for several different types of gravitational-wave detectors (13, 15), most notably bar detectors (16) and laser interferometer detectors (interferometers for short) (17).

An interferometer detector uses four test masses hung by wires near the vertex and ends of an "L" (Fig. 3). The separation L_1 between the two test masses along the first arm is nearly the same as that (L_2) along the second arm, $L_1 \approx L_2 = L$. At frequencies above their pendular swing frequency (about 1 Hz), the test masses move freely horizontally. A gravitational wave (of the appropriate polarization) incident perpendicular to the plane of the interferometer pushes the masses back and forth relative to each other, stretching one arm while squeezing the other, and thereby changing the arm-length difference $\Delta L \equiv L_1 - L_2$. For other directions of incidence, the fractional difference in arm length caused by the wave, $\Delta L/L$, is equal to a linear combination of the two polarization waveforms (13),

$$\frac{\Delta L(t)}{L} = F_+ h_+(t) + F_\times h_\times(t) \equiv h(t) \quad (1)$$

The coefficients F_+ and F_\times are of order

Fig. 2. A general-relativistic gravitational wave propagating in the z direction squeezes and stretches the separation of test particles in a plane perpendicular to the z axis. The wave acts by a combination of its two polarizations: + ("plus") polarization pushes test particles together along the x direction and pushes them apart along the y direction when $h_+(t)$ is positive and it reverses the forces when $h_+(t)$ is negative; \times ("cross") polarization pushes and pulls test particles, as determined by the sign of $h_\times(t)$, at 45° angles from the x and y axes.



unity and depend on the direction to the source and the orientation of the detector. We call $h(t)$ the gravitational-wave strain that acts on the detector. Notice that the relative motion of the test masses caused by the wave is proportional to their initial separation, one of the fundamental facts that drives the design of LIGO.

Laser interferometry is used to monitor ΔL , and thence the gravitational-wave strain $h(t) = \Delta L/L$. In LIGO's first interferometers, the interferometry (18) will be performed as follows (Fig. 3): One face of each test mass is polished and coated to form a mirror with high reflectivity, low transmissivity, and very low scattering and absorption. The two mirrors along each arm form a Fabry-Perot resonant optical "cavity," which gives the effect of having the light traverse the arm many times. A laser beam shines onto a beam splitter at the vertex of the L, and the splitter directs half of the light along each arm, exciting the two Fabry-Perot cavities. The end mirror of each cavity has much lower transmissivity than the mirror near the vertex, so light from each excited cavity exits through its vertex mirror and back toward the beam splitter. The splitter is adjusted to recombine the two returning beams so that most of the recombined light returns toward the laser and a tiny portion propagates toward the photodetector.

When a gravitational wave changes the length L_1 or L_2 of one of the cavities, it slightly shifts the cavity's resonant frequency relative to the laser frequency and thereby changes the phase of the light in the cavity and the phase of the light that exits from the cavity toward the beam splitter. Because the wave affects the two arms differently, it shifts the relative phases of the light exiting the two cavities and thereby alters their interference at the beam splitter, causing a slight change in the intensity at the photodetector. This change in photodetector signal is proportional to $\Delta L(t)$, and thence to the gravitational-wave strain $h(t)$.

The photodetector signal is highly sensitive to $h(t)$, as the following order-of-

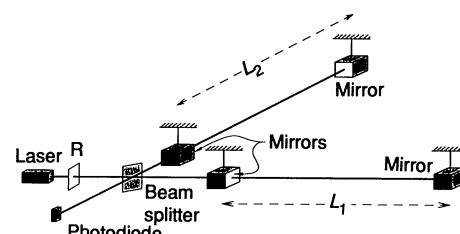


Fig. 3. A schematic view of a LIGO interferometer.

magnitude calculation shows. The relative phase change between the light emerging from the two cavities is

$$\Delta\Phi \approx B \frac{\Delta L}{\lambda} = B \frac{hL}{\lambda} \quad (2)$$

where λ is the light's wavelength and B is the mean number of times the light bounces back and forth in the cavities before exiting (proportional to the cavities' finesse). The phase change $\Delta\Phi$ can be monitored at the photodetector output with a precision that is limited by photon shot noise, that is, by randomness in the arrival times of the photons; the limit is $\Delta\Phi \approx 1/\sqrt{N}$, where N is the number of photons incident on the beam splitter during the time (roughly a gravitational-wave period) that the photodetector's signal is being integrated. Correspondingly, a gravitational-wave strain that would give a signal of the same magnitude as that of the measurement fluctuations is

$$h_{\min} \approx \frac{\lambda}{L} \frac{1}{B} \frac{1}{\sqrt{N}} \quad (3)$$

Actually, $\Delta\Phi$ is proportional to B and h_{\min} is proportional to $1/B$ only if the mean light storage time in the cavities, BL/c , is less than half of a gravitational-wave period (c , speed of light); if B is made larger, there is no further improvement of h_{\min} . For example, the limit is $B \approx 400$, assuming 100-Hz waves and an arm length $L = 4$ km. Given the quality of the LIGO mirrors, only 1% of the photons will be lost to scattering and absorption in the 400 bounces, so almost all of the stored light will exit back toward the laser. This light will be recycled (18) back

into the interferometer by a high-reflectivity mirror placed at the location marked R in Fig. 3. (This makes the entire interferometer a single resonant cavity with arms that are subcavities.) The total power available in the interferometer for making the measurement will then be ~ 100 times as great as the laser's output power. For a laser output of 60 W, this means that $N \approx 2 \times 10^{20}$ photons are incident on the beam splitter during a 10-ms photodetector inte-

gration time. Correspondingly, for the above parameters the minimum detectable wave has a strength (Eq. 3)

$$h_{\min} \approx \left(\frac{0.5 \mu\text{m}}{4 \text{ km}} \right) \left(\frac{1}{400} \right) \left(\frac{1}{\sqrt{2 \times 10^{20}}} \right) \approx 10^{-23} \quad (4)$$

As shown below in Fig. 10, this sensitivity

should be sufficient for the detection of large numbers of gravitational-wave sources and the use of these sources for a rich program of physics and astronomy research.

Several other optical configurations are possible for the interferometer and may be used in future LIGO detectors (19). For example, by inserting a light-recycling mirror between the beam splitter and the photodetector, one can greatly improve the interferometer's sensitivity in a narrow frequency band, while degrading it outside that band (20).

LIGO

LIGO will be a facility open to the national community and capable of housing many successive generations of interferometers with a variety of optical designs. The principal features of LIGO are dictated by the following considerations:

1) Each interferometer's test masses must be housed in a vacuum to avoid buffeting by air molecules. The optical path must also be in vacuum to prevent fluctuations in the number of air molecules in the beam from causing fluctuations in the light's phase. The most sensitive LIGO interferometers will require a vacuum of 10^{-9} torr.

2) An interferometer's sensitivity improves as its arm length L is increased. Achieving sensitivities adequate for the expected waves (Fig. 10 below) requires arms several kilometers in length. LIGO has been designed with 4-km-long arms.

3) The vacuum pipe running between the test masses of each arm will have a diameter of 1.2 m so that it can accommodate multiple detectors as well as auxiliary laser beams required in some advanced detectors (21).

4) To firmly distinguish real gravitational waves from "non-Gaussian" bursts of instrumental and environmental noise, the outputs of interferometers at two widely separated sites will have to be correlated. Three interferometers will be used: a single 4-km interferometer at one site and two interferometers, 4 and 2 km long, sharing the same vacuum system (22) at the other site. If, instead, LIGO were to have only a single vacuum system at a single site, noise bursts would probably prevent its interferometers from recording any meaningful data whatsoever.

5) Each interferometer's test masses must be suspended from vibration isolation systems that protect them from seismic and acoustic vibrations, and the test masses' vacuum chambers must be large enough to house these isolation systems.

6) Before entering the interferometer, the laser light must be conditioned in a variety of ways: it must be frequency-stabi-

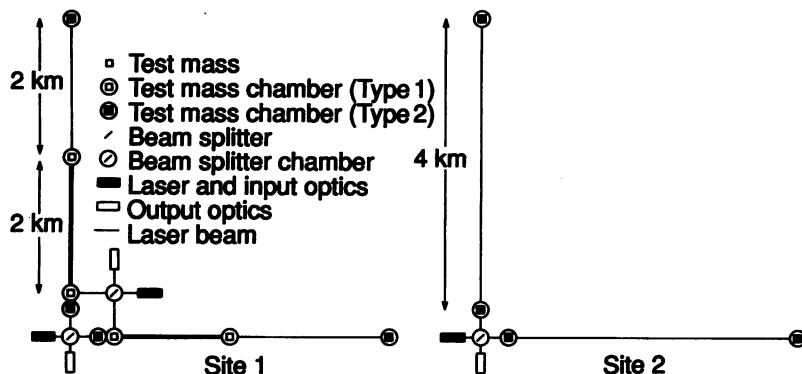
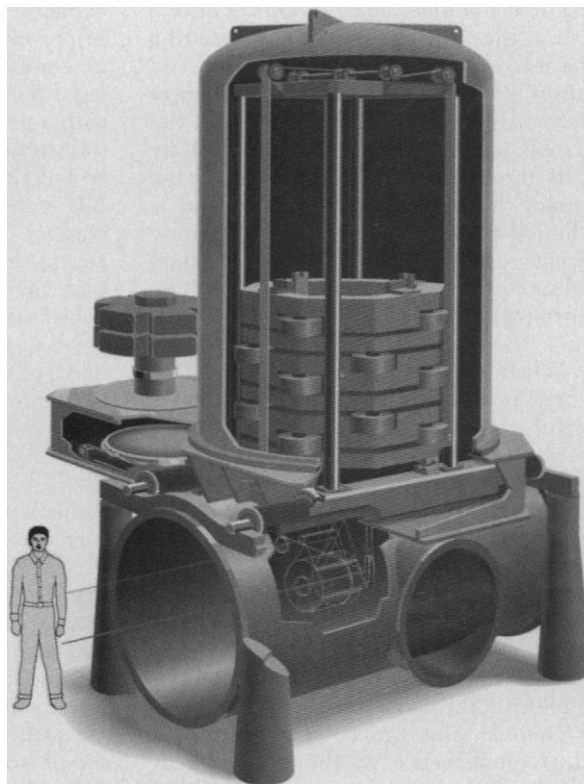


Fig. 4. Schematic layout of the initial LIGO facilities. For each interferometer, the laser beam is conditioned in an input optics chain before it reaches the beam splitter. After passing through the beam splitter, the beams enter the chambers containing the test masses, where they are directed into a 2-km or 4-km interferometer cavity. After leaving the cavity, the beams, now back in the test mass chambers, are directed back to the beam splitter and then into an output optics chain that terminates with the photodetector. At site 1, all elements of the 4-km interferometer lie along the two arms, whereas the beam splitter and input and output optics chains for the 2-km interferometer lie between the two arms.

Fig. 5. An artist's conception of a type 1 LIGO test mass chamber (see the symbols in Figs. 4 and 6), that is, the vacuum system module that houses an interferometer's test masses. The vertical cylinder serves as an air lock that can be opened to the outside from above or, with a horizontal gate valve at its base, opened to the main vacuum pipe below. The large assemblage in the air lock is a passive vibration isolation system (a cascaded stack of mechanical filters consisting of masses and elastomer springs), from which are suspended the test mass and a steering mirror that deflects the light beam from the beam splitter to the test mass and back. The upper laser beam is an auxiliary that monitors the separation between test mass suspension points, so feedback can maintain a fixed separation, thereby helping with vibration isolation (27). The passive vibration isolation system and its suspended test mass and mirror can be raised into the air lock and the gate valve can be closed to permit modifications without interfering with the main vacuum or with other interferometers.



lized, phase-modulated, amplitude-stabilized, and spatially shaped to control various spurious noise sources. This conditioning requires a long input optics chain housed in special vacuum chambers. A similar output optics chain must be placed between the interferometer and the photo-detector.

Figure 4 shows a schematic layout of LIGO's two sites. At site 1 the two interferometers (one 4 km, the other 2 km) are interleaved in such a way that either can be removed from the vacuum system without interfering with the other and without breaking the main vacuum. Figure 5 shows how this capability is designed in the vacuum chambers housing the test masses.

The two LIGO facilities and their first three-interferometer detector system will be constructed from 1992 through 1996 at a cost of ~\$200 million. Subsequent detector systems will cost several million dollars each. The LIGO project is implemented by the "LIGO team," a group of scientists and engineers at the California Institute of Technology (Caltech) and the Massachusetts Institute of Technology, and important contributions are coming from groups at other institutions, including the University of Colorado, Stanford University, and Syracuse University, and from industry.

LIGO's initial configuration is the minimum that can house a three-interferometer detector system capable of detecting the predicted waves and monitoring one of their two waveforms. This initial configuration has been designed to permit an upgrade (presumably after gravitational waves have been detected) into the configuration shown in Fig. 6. The upgraded LIGO can house three independent detector systems that operate simultaneously. These detector systems might be in different stages of development or might be optimized for different types of gravitational waveforms, for example, broadband bursts from black hole collisions or monochromatic waves from pulsars in some chosen narrow-frequency band. From time to time one of the detector systems can be removed and a new one can be inserted in its place, with minimal interference with the other two systems.

Even in this upgraded form, LIGO by itself will not be able to extract all of the information from a gravitational wave [the direction to its source and the two waveforms $h_+(t)$ and $h_\times(t)$]. Full extraction will require combining the outputs of interferometers at three or more widely separated sites, and for all-sky coverage there must be at least four sites (23). LIGO will rely on other nations to provide the third and fourth sites of the network. Vigorous efforts toward doing so are under way in Europe (15) and are being initiated in Japan and

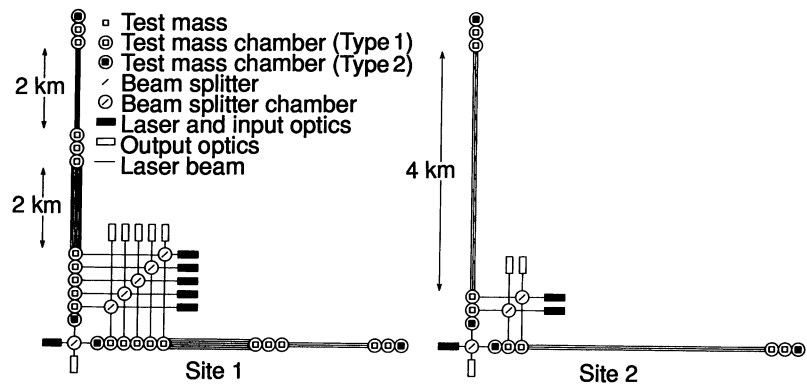


Fig. 6. Schematic layout of the LIGO facilities after a possible future upgrade. Site 1 accommodates three 4-km and three 2-km interferometers without interference, and site 2 accommodates three 4-km interferometers.

Australia (15). The angular resolution of this international network will range from a few arc minutes to a few degrees, depending on the shapes of the waveforms and the signal-to-noise ratio (23). This is comparable to the resolutions of radio telescopes in about 1950, when the first optical identifications of radio sources were being made.

LIGO Interferometers and Their Noise

The noise in any interferometer is of two types: Gaussian (noise with a Gaussian probability distribution) and non-Gaussian. Because of the Gaussian distribution's extremely fast falloff with increasing noise amplitude, Gaussian noise is exceedingly unlikely to produce noise bursts larger than a few standard deviations. By contrast, interferometers can show large, non-Gaussian noise bursts several times per hour due,

for example, to sudden strain releases in the wires that suspend the test masses. The only sure way to remove such non-Gaussian noise in a LIGO detector system is by correlating the outputs of the system's three interferometers. Once this is done, the system's sensitivity will be governed by the remaining, Gaussian noise.

The Gaussian noise is characterized by a spectrum $\hat{h}(f)$ defined as follows. An interferometer's output consists of the true gravitational-wave strain $h(t)$ (Eq. 1) plus the Gaussian noise $h_{\text{noise}}(t)$; $\hat{h}(f)$ is the square root of the power spectral density of $h_{\text{noise}}(t)$ at frequency f . When the interferometer measures a gravitational-wave burst (such as from an inspiraling black hole binary) that has a strain amplitude h_{amp} , a characteristic (mean) frequency f_c , and a duration of n cycles, the measurement, obtained with optimal filter techniques, will have the signal-to-noise ratio (13)

$$\frac{S}{N} \approx \frac{h_c}{h_{\text{rms}}} \quad (5)$$

where

$$h_c \approx h_{\text{amp}} \sqrt{n} \quad (6)$$

is called the wave's characteristic amplitude, and

$$h_{\text{rms}} \equiv \sqrt{f_c} \hat{h}(f_c) \quad (7)$$

is the interferometer's root mean square (rms) noise for a one-cycle-long burst at the source's characteristic frequency f_c (24). [Equations 6 and 7 can be regarded as an approximate definition of the interferometer's noise spectrum $\hat{h}(f)$.]

The LIGO team has developed tentative design parameters for the first LIGO interferometers. (The design will not be finalized until 1993.) A guiding philosophy for this design is that it should use only current technology. These first interferometers are expected to have a Gaussian noise spectrum $\hat{h}(f)$ depicted by the upper solid curve in

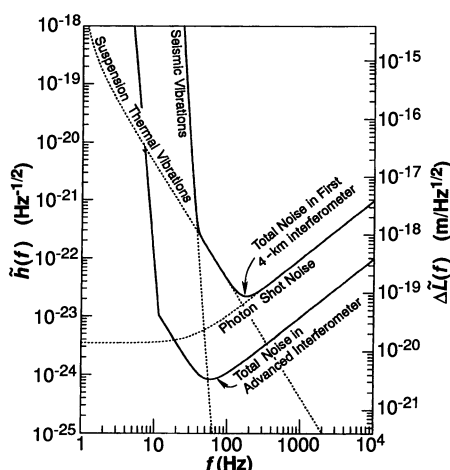


Fig. 7. The expected total noise in each of LIGO's first 4-km interferometers (upper solid curve) and in a more advanced interferometer (lower solid curve). The dashed curves show various contributions to the first interferometer's noise.

Fig. 7. The individual contributions to this noise, shown as dashed curves, arise from the following sources:

1) Below ~ 70 Hz, the total noise (upper solid curve) will be dominated by "seismic noise" (ground vibrations due to the seismic background, to man-made sources such as traffic on roads or railroads, or to wind forces coupled to the ground by trees and buildings), which is transmitted to the test masses through their suspensions. The test masses will be protected from such noise by a passive seismic isolation system (Fig. 5) and the final pendulum suspension. The seismic noise limit is very steep because such a vibration isolation system loses its effectiveness at low frequencies.

2) Between ~ 70 and ~ 200 Hz, the noise is predominately due to off-resonance, thermally induced vibrations of the

test masses and their suspensions. These thermal vibrations will produce the noise shown in Fig. 7, assuming 10-kg test masses and a 10^7 quality factor for their pendulum suspensions.

3) Above ~ 200 Hz, photon shot noise will dominate. This is the type of noise discussed in the text preceding Eq. 3. The curve shown in Fig. 7 is based on the assumptions of 2 W of effective laser power [comparable to that of existing argon ion lasers or to frequency-doubled neodymium:yttrium-aluminum-garnet (Nd:YAG) lasers that are being developed by the LIGO team's Stanford collaborators], mirrors with a fractional power loss of 5×10^{-5} per reflection (which has been demonstrated in smaller mirrors, but not yet in the 20-cm size required for LIGO), and a factor of 30 gain in effective laser power by light recycling [comparable with what has been demonstrated in interferometers with fixed mirrors (25)].

A number of other noise sources must be controlled; all are expected to be less important than these three.

Throughout LIGO's operation, its interferometers will be continually improved. The lower solid curve of Fig. 7 depicts the noise in a candidate next-generation advanced interferometer. (The technology and techniques for this and other advanced interferometers are now under development.) This advanced interferometer's noise reduction would be largely achieved in three ways: (i) To reduce the photon shot noise, the effective laser power would be increased to 60 W and the mirror losses would be improved to permit recycling the light 100 rather than 30 times. (The resulting rms shot noise, $h_{\text{rms}} = \sqrt{f} \dot{h}(f)$ at $f = 100$ Hz, is 10^{-23} , in accord with the estimate in Eq. 4.) (ii) To reduce the pendulum suspensions' thermal vibrations, their quality factor would be increased from 10^7 to 10^9 by a change in their material and geometry, and the test masses would be increased from 10 to 1000 kg. (iii) To reduce the seismic vibrations, the isolation stack would be upgraded, and an active isolation system (26, 27) might be used.

Prototype Interferometer Development

The designs of the first and advanced LIGO interferometers and the confidence that their expected noise levels can be achieved are the result of extensive experiments carried out over the past decade in the LIGO team's laboratories and elsewhere. These experiments have separately tested various performance requirements and interferometer components. The predicted performance of LIGO interferometers must be pieced together from these individual experiments without any unified demonstration, because laboratory-scale interferometers are significantly different from 4-km LIGO interferometers—different because various noise sources scale differently with increasing arm length and changing frequency.

One of the key instruments being used in the development and testing of components and techniques for full-scale LIGO interferometers is a 40-m prototype at Caltech (Fig. 8). Experiments with this prototype (28) have tested a variety of interferometer components and a wide range of their performance measures; Fig. 9 shows measurements of displacement noise, $\Delta \tilde{L}(f)$. $[\Delta \tilde{L}(f)]$ is the square root of the power spectral density of ΔL and is related to $\dot{h}(f)$ by

$$\Delta \tilde{L}(f) = L \dot{h}(f) \quad (8)$$

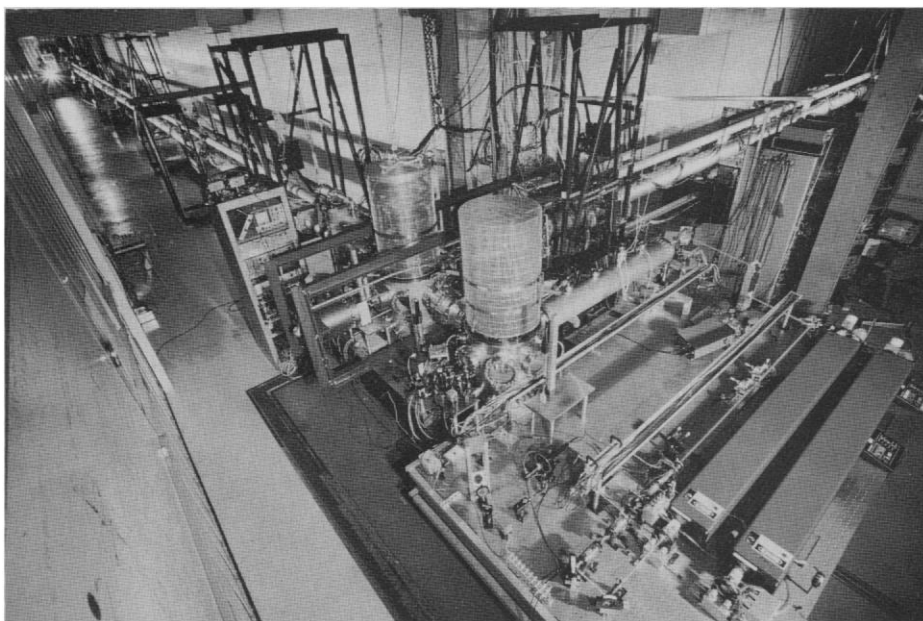


Fig. 8. A photograph of the 40-m prototype interferometer at Caltech.

Fig. 9. The displacement noise achieved by 40-m prototype interferometers at various times in the past, and comparison with the estimated displacement noise in the first LIGO interferometers (see Fig. 7 and Eq. 8). The lines of constant h_{rms} were computed from Eqs. 7 and 8 with the prototype arm length, $L = 40$ m (or, in parentheses, the LIGO arm length, $L = 4$ km).

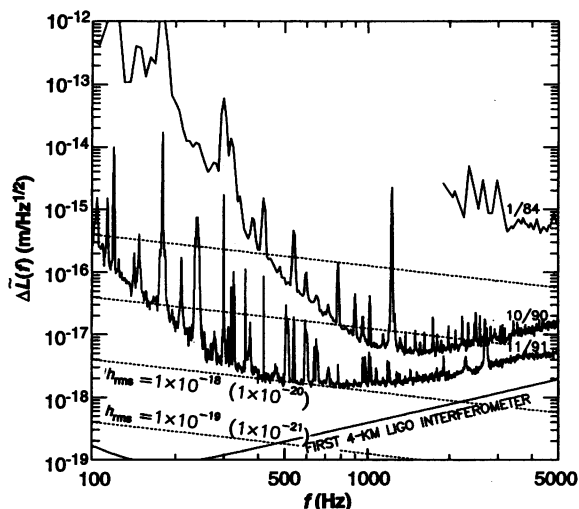
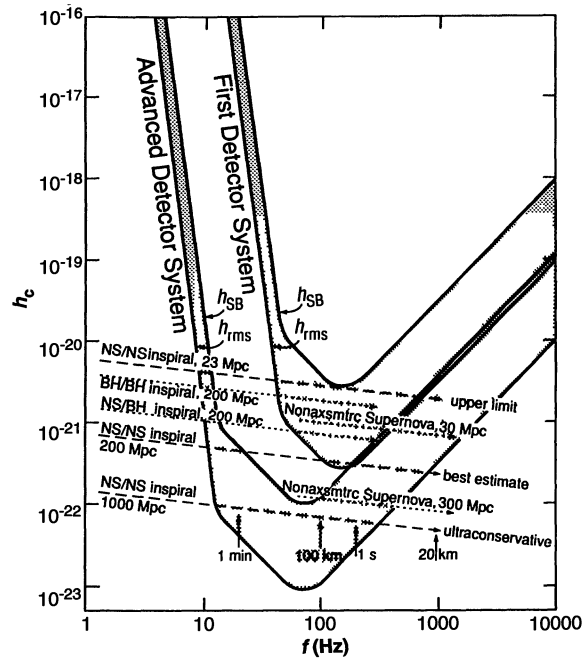


Fig. 10. Comparison between the expected rms noise h_{rms} in LIGO's first and advanced detector systems and the characteristic amplitude h_c of gravitational-wave bursts from several hypothesized sources. NS, neutron star; BH, black hole.



See Eqs. 1 and 7.] The bottom spectrum in Fig. 9 is the prototype's displacement performance in November 1991. Long-term prototype progress is shown by a comparison with the January 1984 spectrum, and recent shorter term progress is shown by a comparison with the October 1990 spectrum. Also shown is the displacement noise expected in LIGO's first 4-km interferometers.

The 1991 spectrum shows a number of peaks superimposed on a smooth background. Some of the low-frequency peaks are due to imperfections in electromechanical servos, and the largest peaks at higher frequency are due to mechanical resonances in an intermediate reference cavity. All of these peaks can be removed with further work, leaving only peaks due to thermally excited vibrational modes of the test masses' suspension wires (the clusters of peaks near 330, 500, and 650 Hz). Even in its present state, the spectrum's baseline level, not the peaks, is the more accurate measure of the detector's displacement sensitivity, because narrow peaks can be filtered out in the data analysis with minimal loss in signal.

The baseline noise is due to a number of different sources. At high frequencies (above ~ 1 kHz), the noise is dominated by shot noise and is consistent with the level predicted for the current laser power and interferometer optical configuration. At very low frequencies (below ~ 120 Hz), the observed noise is due to ground vibrations that couple through the suspensions to the test masses. The level of this noise component is somewhat higher than the LIGO goal, in part because of the ground vibra-

tion level in the Caltech laboratory, which is a factor of 10 higher than measured levels at remote sites more representative of probable LIGO sites. In the intermediate region, the noise spectrum contains contributions from a number of sources, the relative importance of which varies with frequency. In addition to seismic noise and shot noise, there are significant contributions from thermal noise and from scattered light that recombines and interferes with the main laser beam. All of these noise sources can be reduced with further work. For example, the level of noise due to scattered light is highly dependent on the detailed configuration of the interferometer; because of space constraints within its current vacuum chamber, the 40-m prototype does not contain many of the measures planned for the first LIGO interferometers to control scattered light.

Experiments performed on the 40-m prototype and other special purpose setups have (i) tested and confirmed the photon shot noise formula used to predict the noise spectra of LIGO interferometers; (ii) tested the formula for the noise from residual gas and confirmed the vacuum requirement in the beam tubes; (iii) demonstrated the effective power enhancement due to recycling in a Fabry-Perot interferometer (25); and (iv) allowed the development of a technique for laser stabilization (29) and verified that sufficient frequency stability can be achieved for the first LIGO interferometers.

Taken together, these separate experiments, and others performed in other laboratory facilities, give us confidence that the fundamental noise sources are under-

stood and that the LIGO noise performance goals of Fig. 7 can be achieved. However, a final demonstration of all aspects of the LIGO detectors' performance must await the 1996 installation of the first detector system in the full-scale LIGO facilities.

Comparison of LIGO Sensitivities with Estimated Wave Strengths

LIGO's first detector system might see gravitational waves, and the advanced detectors discussed above are highly likely to see them. Success will probably come between the first-detector level and the advanced level, that is, a few years after LIGO goes into operation.

This prediction is based largely on the best understood of the hypothesized sources: the final, minute-long inspiral of a neutron star binary. Because the 10-km-sized stars are 100 km apart when LIGO is most sensitive to them, they are not yet tearing each other apart, and the details of their wave emission are understood (13, 30, 31). The uncertainty in the waves' strength arises solely from the uncertain distance to the nearest such sources. The observed statistics of binary neutron stars in our own galaxy, extrapolated to include distant galaxies, give a best estimate (32, 33) of 200 Mpc (650 million light years) for the distance to which LIGO must look to see three neutron star inspirals per year. Further analysis (32) of the uncertainties in the data gives an "ultraconservative upper limit" of 1000 Mpc and an "optimistic lower limit" of ~ 23 Mpc.

Figure 10 shows the characteristic amplitudes h_c (Eq. 6) of the waves from neutron star binaries at these three distances (34). The waves sweep with time from low frequency to high, that is, from left to right in Fig. 10 (see waveform in Fig. 1). As the frequency increases, the waves' amplitude h_{amp} increases; however, the number of cycles $n = f^2(df/dt)^{-1}$ spent near each frequency f decreases, and the characteristic amplitude $h_c \approx h_{amp}\sqrt{n}$ (which determines the signal-to-noise ratio) decreases slightly (see dashed arrows in Fig. 10). (The vertical arrows along the bottom of Fig. 10 mark the remaining times, 1 min and 1 s, until the final neutron star collision, and the distances, 100 km and 20 km, between the stars.)

Figure 10 allows a comparison of these signal strengths with the expected noise in the first and advanced LIGO detectors. The lower curve of each pair is the rms noise h_{rms} (Eq. 7) in each 4-km interferometer, as computed from the noise estimates of Fig. 7. The upper curve in each pair is the sensitivity to bursts,

$$h_{SB} = 11h_{rms} \quad (9)$$

that is, the strength h_c that a burst must have—if it arrives only rarely, from a random direction, with an arbitrary polarization, and at a random, unpredictable time—in order for us to be highly confident that it is not due to Gaussian noise (35). [If the neutron stars' final collision produces a strong enough burst of gamma rays for detection at Earth (36), then the gamma burst will dictate the time at which to expect the gravitational-wave burst, and the waves can then be identified with confidence at $h_c \approx h_{SB}/3$, that is, a factor of 3 below the upper curve in each pair.]

Figure 10 shows that LIGO's first detectors will be about good enough to detect three neutron star inspiral events per year at the "optimistic" level, and the advanced detectors will be about good enough at the "ultraconservative" level. Most likely, the first detection will be somewhere in between.

The first detection can be used for waveform studies (Fig. 1), even if it barely exceeds the detectors' burst sensitivity h_{SB} , because h_{SB} is far above the interferometers' rms noise (35). Each factor of 2 sensitivity improvement thereafter not only will improve the accuracies of waveform studies, but also will increase the rate of observed signals by a factor $2^3 = 8$, because the event rate scales with volume, that is, is proportional to h_{SB}^{-3} . Correspondingly, if three neutron star inspirals occur each year at 200 Mpc (the best estimate), then the rate will be about one event every 2 to 3 days in the advanced detector system.

Figure 10 also shows, at 200 Mpc [the best current estimate for how far LIGO must look to see three such events per year (32, 33)], the waves from a neutron star spiraling into one ~ 10 -solar mass black hole and from two ~ 10 -solar mass black holes spiraling together. Although the three-per-year distance for these sources is much less certain than that for neutron star binaries, the waves at a given distance are stronger—so strong, in fact, that the advanced detector system could see the inspiral of black hole binaries throughout the universe (out to cosmological distances, where the event rate should be $\sim 10,000$ times as high as that at the best-estimate distance of 200 Mpc, or several events per hour).

Figure 1 shows how LIGO can allow researchers to infer, from the inspiral waveforms, the details of the binary's orbits and the masses of its black holes or neutron stars. In the last second of the binary's life, its inspiral waveforms gradually give way to collisional, merger, or tidal-disruption waveforms (depending on the nature of the binary), from which one can extract fundamental physics—(i) from the final collision of comparable-mass holes: details of the

poorly understood, highly nonlinear dynamics of space-time curvature (10); (ii) from the inspiral of a small hole into a large hole: a detailed, partial map of the large hole's curvature (8, 9); (iii) from the tidal disruption of a neutron star by its companion black hole: the neutron star's radius (which, combined with its measured mass, will give information about the equation of state of nuclear matter); and (iv) from the collision of two neutron stars: their collisional dynamics and perhaps their radii. For two neutron stars, the collisional waveform will be concentrated at frequencies of 500 to 1000 Hz, where the detectors' photon shot noise is severe; so studying the collision will require specialized detectors with enhanced high-frequency sensitivity (and consequently reduced low-frequency performance). For binaries containing two black holes more massive than about ten suns, by contrast, the final waveform may be at low enough frequencies for study with the broadband, advanced detectors of Fig. 10.

Of course, coalescing binaries are not the only potential gravitational-wave sources for LIGO. There are others (14): rotating, slightly nonaxisymmetric neutron stars; collapsing stellar cores (as for example, in supernovae); stochastic waves from vibrating cosmic strings and from the big bang; and, of course, totally unexpected types of sources. However, these other sources are all uncertain in wave strength, event rate, or both.

One example is a nonaxisymmetric supernova. Type II supernovae are known to be triggered by the collapse of a star's core to form a neutron star (37). If the collapse is axially symmetric, then the gravitational waves emitted will be too weak to detect beyond our galaxy and the Magellanic Clouds (38). On the other hand, if the core is spinning sufficiently fast, then centrifugal forces may halt its collapse at radii of several hundred kilometers, and an instability then might [but theory has not yet confirmed this (39)] drive the flattened, spinning core into a nonaxisymmetric shape, so it tumbles like a football turning end over end and emits strong gravitational waves. If it is the gravitational waves, and not hydrodynamic waves, that carry off most of the core's excess angular momentum, thereby permitting it to shrink to neutron star size (~ 10 km), and if 10% of type II supernovae are triggered by such collapses, then the distance to which one must look to see three such events per year is ~ 30 Mpc (40) and the wave strength is roughly that shown in Fig. 10 (41). Reducing the fraction of type II supernovae that undergo such collapses by a thousand (to 0.01%) would increase the distance one must look to 300 Mpc. It may well be that such nonaxisymmetric supernovae never

occur in nature, or they may occur so rarely that LIGO will never see one. However, there is an observational hint of strong asymmetry in the recent discovery of a neutron star that seems to have been ejected at 1/100th of the speed of light from the center of its supernova explosion (42).

This discussion of nonaxisymmetric supernovae, with all its "ifs" and "mights," illustrates the enormous uncertainties that plague estimates of the gravitational waves from most astrophysical objects. The greatest hope for resolving the uncertainties is to search for the waves, and, when they are found, to study their waveforms.

Conclusions

The fiscal year 1992 National Science Foundation budget contains the first portion of LIGO's $\sim \$200$ -million construction cost. The selection of the two LIGO sites is now entering its final stage, and the sites should be in hand and the construction begun at the first site by the end of 1992. If future funding is granted at the planned rate, construction at the two sites will be completed in 1995 and 1996, the facilities will have been checked out and begun operation by the end of 1997, and the first detector system will be operational in 1998.

This first detector system may discover gravitational waves. If not, experimenters will press forward with detector improvements (for which development is already under way), leading toward LIGO's advanced detector goals. These improvements are expected to lead to the detection of waves from many sources each year. The scientific community can then begin to harvest the rich information carried by the waves, and an upgrade of LIGO can make it possible for several research groups simultaneously to operate several different detector systems, each optimized for a different type of astrophysical source.

Note added in proof: While this paper was in press, the National Science Foundation selected the two LIGO sites from among 19 proposals. The selected sites are Livingston, Louisiana, and Hanford, Washington.

REFERENCES AND NOTES

1. See, for example, C. W. Misner, K. S. Thorne, J. A. Wheeler, *Gravitation* (Freeman, San Francisco, 1973).
2. See, for example, I. D. Novikov and V. P. Frolov, *Physics of Black Holes* (Kluwer Academic, Dordrecht, Netherlands, 1989), and references therein.
3. See, for example, J. D. Barrow, *Phys. Rep.* **85**, 1 (1982).
4. J. H. Taylor and J. M. Weisberg, *Astrophys. J.* **345**, 434 (1989), and references therein.
5. See, for example, C. M. Will, *Theory and Experiment in Gravitational Physics* (Cambridge Univ. Press, Cambridge, 1981).

6. D. M. Eardley *et al.*, *Phys. Rev. Lett.* **30**, 884 (1973); D. M. Eardley, D. L. Lee, A. P. Lightman, *Phys. Rev. D* **8**, 3308 (1973).

7. K. S. Thorne, in *Gravitational Radiation*, N. Deruelle and T. Piran, Eds. (North-Holland, Dordrecht, Netherlands, 1983), pp. 1–54.

8. L. S. Finn, A. Ori, K. S. Thorne, in preparation.

9. S. L. Detweiler, *Astrophys. J.* **225**, 687 (1978); _____ and E. Szedenits, *ibid.* **231**, 211 (1979); T. Nakamura, K. Oohara, Y. Kojima, *Prog. Theor. Phys. (suppl.)* **90**, 1 (1987).

10. See, for example, C. R. Evans, L. S. Finn, D. W. Hobill, Eds., *Frontiers in Numerical Relativity* (Cambridge Univ. Press, Cambridge, 1989); G. B. Cook and J. W. York, *Phys. Rev. D* **41**, 1077 (1989); J. Bowen, J. Rauber, J. W. York, *Class. Quantum Gravity* **1**, 591 (1984); L. Smarr, *Ann. N.Y. Acad. Sci.* **301**, 569 (1977).

11. See, for example, S. L. Shapiro and S. A. Teukolsky, *Black Holes, White Dwarfs, and Neutron Stars* (Wiley, New York, 1983).

12. For the history of radio astronomy and the revolution it brought, see K. Kellermann and B. Sheets, Eds., *Serendipitous Discoveries in Radio Astronomy* (National Radio Astronomy Observatory, Green Bank, WV, 1983); W. T. Sullivan, Ed., *Classics in Radio Astronomy* (Kluwer, Dordrecht, Netherlands, 1982); *The Early Years of Radio Astronomy* (Cambridge Univ. Press, Cambridge, 1984).

13. K. S. Thorne, in *300 Years of Gravitation*, S. W. Hawking and W. Israel, Eds. (Cambridge Univ. Press, Cambridge, 1987), pp. 330–458.

14. For discussions and lists of references, see (13) and K. S. Thorne, in *Recent Advances in General Relativity*, A. Janis and J. Porter, Eds. (Birkhauser, Boston, 1992), pp. 196–229.

15. D. G. Blair, Ed., *The Detection of Gravitational Waves* (Cambridge Univ. Press, Cambridge, 1991).

16. Bar detectors were invented by J. Weber [*Phys. Rev.* **117**, 306 (1960)] and have been developed to a high degree of sophistication since then; see, for example, P. F. Michelson, J. C. Price, R. C. Taber, *Science* **237**, 150 (1987); (15).

17. The seeds of the idea for laser interferometer gravitational-wave detectors are contained in F. A. E. Pirani, *Acta Phys. Pol.* **15**, 389 (1956), in M. E. Gertsenshtein and V. I. Pustovoit, *Sov. Phys. JETP* **16**, 433 (1963), and in J. Weber's personal notebooks from the 1960s; the first detailed descriptions of the idea were by G. E. Moss, L. R. Miller, and R. L. Forward [*Appl. Opt.* **10**, 2495 (1971)] and by R. Weiss [*Quart. Prog. Res. Lab. Electron. M.I.T.* **105**, 54 (1972)].

18. R. W. P. Drever, in *Gravitational Radiation*, N. Deruelle and T. Piran, Eds. (North-Holland, Dordrecht, Netherlands, 1983), pp. 321–338; R. W. P. Drever *et al.*, in *Quantum Optics, Experimental Gravity, and Measurement Theory*, P. Meystre and M. O. Scully, Eds. (Plenum, New York, 1983), pp. 503–514, and references therein.

19. For example, the two arms can be operated as optical delay lines, with the bouncing light in them making many discrete spots on the mirrors instead of being trapped in a Fabry-Perot cavity [R. Weiss, in (17)]. This configuration is now being developed in Europe (15).

20. B. J. Meers, *Phys. Rev. D* **38**, 2317 (1988); K. A. Strain and B. J. Meers, *Phys. Rev. Lett.* **66**, 1391 (1991); and references therein.

21. The many laser beams in each arm may include (i) up to six simultaneous Fabry-Perot cavity beams after an upgrade of LIGO's corner and end stations, (ii) beams connecting the suspension points of the test masses (27) as part of seismic isolation systems (see Fig. 5 for an example); and (iii) the many individual beams of a single interferometer with arms that are optical delay lines rather than Fabry-Perot cavities (19).

22. Some noise sources will be common to the vacuum-sharing 4- and 2-km interferometers. However, many will not be common, and those that are will typically not mimic a true gravitational wave's 2:1 ratio of signal strengths.

23. Y. Gürsel and M. Tinto, *Phys. Rev. D* **40**, 3884 (1990).

24. Similarly, when used in the study of periodic

waves (such as from a pulsar) with amplitude h_{amp} and frequency f , the interferometer will have the signal-to-noise ratio (13)

$$\frac{S}{N} = \frac{h_{\text{amp}} \sqrt{\tau_{\text{int}}}}{\hbar(f)}$$

where τ_{int} is the total time over which the periodic signal is integrated.

25. P. Fritschel, D. Shoemaker, R. Weiss, *Appl. Opt.*, in press.

26. R. L. Rinker and J. E. Faller, in "Precision instruments and fundamental constants II," B. N. Taylor and W. D. Phillips, Eds., *National Bureau of Standards Spec. Pub.* **617**, 411 (1984); N. A. Robertson *et al.*, *J. Phys. E* **15**, 1101 (1982); P. R. Saulson, *Rev. Sci. Instrum.* **15**, 1315 (1984); N. A. Robertson, in *The Detection of Gravitational Waves*, D. Blair, Ed. (Cambridge Univ. Press, Cambridge, 1990), pp. 353–368.

27. R. W. P. Drever, in *The Detection of Gravitational Waves*, D. Blair, Ed. (Cambridge Univ. Press, Cambridge, 1990), pp. 306–328.

28. A technical description of the prototype and experiments that have been carried out with it will be published soon.

29. R. W. P. Drever *et al.*, *Appl. Phys.* **B31**, 97 (1983).

30. B. F. Schutz, *Nature* **323**, 310 (1986); *Class. Quantum Gravity* **6**, 1761 (1989); H. D. Wahlquist, *Gen. Relativ. Gravit.* **19**, 1101 (1987).

31. C. W. Lincoln and C. M. Will, *Phys. Rev. D* **42**, 1123 (1990).

32. E. S. Phinney, *Astrophys. J.* **380**, L17 (1991).

33. R. Narayan *et al.*, *ibid.* **379**, L17 (1991).

34. From equation 46b of (7), with a $\sqrt{2}$ correction added because of the incorrect use of ft rather than $\int (d/dt)dt$ in equation 42 of (7), and with neutron star masses of 1.4 solar masses.

35. Because the burst is far out on the tail of the noise's Gaussian probability distribution, h_{SB} is quite insensitive to whether the time between bursts is 1 month or 1 year and to whether by "highly confident" one means 90% or 99%. The factor 11 in Eq. 9 is made up of (i) a factor of $\sqrt{5}$ that is included because, owing to the detectors' quadrupolar beam pattern, waves from a random (typical) direction produce a signal $\sqrt{5}$ times as small as that from an optimal direction and (ii) a factor of 5 from the Gaussian statistics for two identical 4-km interferometers that search for events of duration ~ 0.01 s that occur a few times per year. See (13) for a more careful analysis and discussion; in that reference h_{SB} is called $h_{3\text{Myr}}$.

36. P. Haensel, B. Paczynski, P. Amsterdamski, *Astrophys. J.* **375**, 209 (1991).

37. See, for example, S. E. Woosley and T. A. Weaver, *Annu. Rev. Astron. Astrophys.* **24**, 205 (1986).

38. R. Mönchmeyer, G. Schäfer, E. Müller, R. E. Kates, *Astron. Astrophys.* **246**, 417 (1991); L. S. Finn, *Ann. N.Y. Acad. Sci.* **631**, 156 (1991).

39. See, for example, the following references for discussion of this so-called "bar mode instability" in various contexts: S. Chandrasekhar, *Ellipsoidal Figures of Equilibrium* (Yale Univ. Press, New Haven, CT, 1969); J. R. Ipser and L. Lindblom, *Phys. Rev. Lett.* **62**, 2777 (1989); *Astrophys. J.* **355**, 226 (1990).

40. For the rates of supernova explosions, see S. van den Bergh and G. A. Tammann, *Annu. Rev. Astron. Astrophys.* **29**, 363 (1991).

41. This wave strength h_c is independent of the strength of the instability and the resulting degree of nonaxisymmetry as long as the gravitational waves are responsible for carrying away the core's angular momentum. For weaker instabilities, the waves' amplitude h_{amp} is smaller and the number of cycles n that the waves spend near a frequency f is larger; the product $h_c = h_{\text{amp}} \sqrt{n}$ is constant.

42. D. A. Frail and S. R. Kulkarni, *Nature* **352**, 785 (1991).

43. This work was supported in part by NSF grant PHY-8803557.

Global Tectonics and Space Geodesy

Richard G. Gordon and Seth Stein

Much of the success of plate tectonics can be attributed to the near rigidity of tectonic plates and the availability of data that describe the rates and directions of motion across narrow plate boundaries ~ 1 to 60 kilometers wide. Nonetheless, many plate boundaries in both continental and oceanic lithosphere are not narrow but are hundreds to thousands of kilometers wide. Wide plate boundary zones cover ~ 15 percent of Earth's surface area. Space geodesy, which includes very long baseline radio interferometry, satellite laser ranging, and the global positioning system, is providing the accurate long-distance measurements needed to estimate the present motion across and within wide plate boundary zones. Space geodetic data show that plate velocities averaged over years are remarkably similar to velocities averaged over millions of years.

Plate motion, Earth's most important tectonic process, was first quantitatively described about 25 years ago (1, 2). Earth's strong outer layer that composes the plates is termed the lithosphere, which typically comprises the crust plus the uppermost mantle and is of variable thickness but may

typically be ~ 100 km thick. The presumably much weaker layer immediately below the lithosphere is termed the asthenosphere. Plate tectonics is the culmination of the hypothesis of seafloor spreading (3). That geomagnetic reversals are recorded by the seafloor as it spreads away from mid-ocean ridges (4) made possible the confirmation of seafloor spreading and the estimation of seafloor spreading rates (5).

The authors are in the Department of Geological Sciences, Northwestern University, Evanston, IL 60208.